



# Evolution of Entropy and Mediation of the Solar Wind by Turbulence

L. Adhikari<sup>1</sup> , G. P. Zank<sup>1,2</sup> , L.-L. Zhao<sup>1</sup> , and G. M. Webb<sup>1</sup> <sup>1</sup> Center for Space Plasma and Aeronomic Research (CSPAR), University of Alabama in Huntsville, Huntsville, AL 35899, USA<sup>2</sup> Department of Space Science, University of Alabama in Huntsville, Huntsville, AL 35899, USA

Received 2019 December 4; revised 2020 January 22; accepted 2020 January 23; published 2020 March 2

## Abstract

We study the evolution of solar wind entropy based on a conservative formulation of solar wind and turbulence transport model equations, and compare the model results to *Voyager 2* measurements. For a polytropic index of  $\gamma = 5/3$  ( $>1$ ), entropy increases with distance due to the dissipation of turbulence, being about 12.84% higher at 75 au than at 1 au. However, if the polytropic index satisfies  $\gamma < 1$ , entropy decreases. We show that not only the creation of pickup ions, but also stream-shear leads to a decrease of the solar wind speed. We show that the sum of the solar wind flow energy (kinetic plus enthalpy) and turbulent (magnetic) energy is constant, indicating that kinetic solar wind energy is transferred into turbulent energy via stream-shear and pickup ion isotropization, which then in turn heats the solar wind via the dissipation of turbulence. We compare the theoretical solutions of the solar wind entropy, the solar wind density, the thermal gas pressure, the solar wind proton temperature, and the fluctuating magnetic energy with those measured by *Voyager 2*. The results show that the theoretical results are in good agreement with the observed results.

*Unified Astronomy Thesaurus concepts:* [The Sun \(1693\)](#); [Solar wind \(1534\)](#); [Interplanetary turbulence \(830\)](#)

## 1. Introduction

Entropy is an important thermodynamic property of solar wind. For a simple magnetohydrodynamic (MHD) model with scalar pressure (hence isotropic temperature), the entropy is defined as  $S = c_v \log(P/\rho^\gamma)$ , where  $P(=2nk_B T)$  is the thermal pressure,  $n(\rho)$  is the solar wind (mass) density,  $T$  is the solar wind proton temperature,  $k_B$  is the Boltzmann constant,  $\gamma$  is a polytropic index, and  $c_v$  is a specific heat constant. The entropy formula  $S(=c_v \log(P/\rho^\gamma))$  is related to the Maxwellian distribution. For a kappa distribution, the entropy formula  $S_\kappa$  is slightly different, being given instead by  $S = \log[1 - (1/\kappa)S_\kappa/k_B]^{-\kappa}$ , where  $\kappa$  is the kappa index, and  $k_B$  is Boltzmann's constant (Livadiotis 2018b). There can be a positive or negative correlation between solar wind proton temperature and solar wind density, which affects the evolution of the solar wind entropy. The proton temperature is positively correlated with the solar wind density near and inside 1 au, and negatively correlated with the solar wind density outside  $\sim 20$  au (Whang et al. 1989, 1990; Adhikari et al. 2014; Livadiotis 2018a; Zank et al. 2018b). For adiabatic, isothermal, and isochoric processes, the polytropic index  $\gamma$  equals  $5/3$ ,  $1$ , and  $\infty$ , respectively. When the polytropic index approaches zero, the process is called isobaric. For example, it is found that the polytropic index becomes zero in planetary magnetosheaths (Nicolaou et al. 2015) and the inner heliosheath (Livadiotis & McComas 2012, 2013). Many studies have shown that the polytropic index usually ranges from 0.5 to 2.5, with 1.66 as the center, equivalent to  $5/3$  (Nicolaou et al. 2014; Livadiotis & Desai 2016; Livadiotis 2018a). In our study, we use  $\gamma = 5/3$ .

Whang et al. (1989, 1990) studied the evolution of entropy between 0.3 and  $\sim 30$  au using *Helios A*, *Helios B*, *Voyager 2*, *Voyager 1*, *Pioneer 10*, and *Pioneer 11* measurements and MHD simulations. When a typical shock wave propagates through the solar wind, the entropy of the solar wind protons increases by about  $0.8 \times 10^{-23}$  J/K/proton due to shock wave heating (Whang et al. 1990; see also, Anand & Yadav 2014;

Fahr & Siewert 2015). The Whang et al. result shows that solar wind entropy increases with heliocentric distance, such that when the heliocentric distance increases 10 times, the entropy increases by about  $4 \times 10^{-23}$  J/K/proton (Whang et al. 1990).

In this paper, an entropy transport equation with turbulent heating as the source term is derived, and the evolution of entropy in the outer heliosphere between 1 and 75 au is studied. We use a simple turbulence model to derive the source term for the entropy transport equation (see Appendix, and also Zank et al. 1996, 2012). In the Appendix, we derive coupled turbulence transport model equations for the fluctuating magnetic energy density and the correlation length for two cases corresponding to (i) when the solar wind turbulence is mainly dominated by the fluctuating magnetic energy, and (ii) when pickup ion (PUI) driven turbulence excites Alfvén waves in the outer heliosphere. We then derive a conservative form of the coupled solar wind and turbulence transport equation that conserves the total energy flux (i.e., the sum of the solar wind energy flux and the turbulent magnetic energy flux).

Previous studies have shown the importance of turbulence in understanding (i) solar wind acceleration and coronal plasma heating to millions of degrees of Kelvin (Matthaeus et al. 1999a; Viñas et al. 2000; Dmitruk et al. 2001, 2002; Oughton et al. 2001; Suzuki & Inutsuka 2005; Cranmer et al. 2007, 2013; Chandran & Hollweg 2009; Chandran et al. 2010; Cranmer & van Ballegoijen 2010; Verdini et al. 2010; Usmanov et al. 2011; van Ballegoijen et al. 2011; Woolsey & Cranmer 2014; van Ballegoijen & Asgari-Targhi 2016; Zank et al. 2018a), (ii) solar wind heating (Matthaeus et al. 1999b; Smith et al. 2001, 2006; Breech et al. 2008; Adhikari et al. 2014, 2015, 2017; Wiengarten et al. 2016; Shiota et al. 2017; Zank et al. 2017, 2018b), and (iii) the propagation of cosmic rays throughout the heliosphere (Zank et al. 1998; Chhiber et al. 2017; Zhao et al. 2017, 2018). This paper reveals the role of turbulence in the evolution of solar wind entropy. We organize the paper as follows. We present the theoretical model in Section 2, discuss our results in Section 3, and summarize our results in Section 4.

## 2. Theoretical Model Equations

Various in situ effects in the large-scale solar wind extract energy and momentum from large-scale flow. Perhaps the best known example is the deceleration of the supersonic solar wind in the outer heliosphere as a consequence of the pick up of interstellar neutral gas, primarily hydrogen, in the outer heliosphere. However, other large-scale processes, such as the interaction of fast and slow wind and associated stream-shear instabilities extract energy and momentum from the solar wind, which must result in its deceleration. It is now recognized that, despite the complications of solar cycle variation and interplanetary shock waves, the creation of PUIs causes the solar wind speed to decrease gradually in the outer heliosphere (Richardson & Smith 2003; Zank et al. 2018b; Elliott et al. 2019). The evolution of the solar wind speed is determined by a 1D steady-state momentum equation in the form,

$$\rho U \frac{dU}{dr} = -\frac{dP}{dr} - \frac{\rho}{U} S^{\text{shear}} - \frac{\rho}{U} S^{\text{PUI}}. \quad (1)$$

The variable  $U$  is the solar wind speed,  $\rho$  is the solar wind mass density, and  $P$  is the thermal gas pressure. The first term on the right-hand side (rhs) of Equation (1) is the pressure gradient, the second term is related to the stream-shear instability driven by the inhomogeneous solar wind flow, and the third term is related to the loss of momentum of the solar wind flow resulting from the creation of PUIs. The second and third terms on the rhs ( $S^{\text{shear}}$  and  $S^{\text{PUI}}$ ) are derived below. Equation (1) shows that the solar wind speed decreases because both stream-shear and PUI creation extract momentum (and energy) from the supersonic flow (e.g., Richardson & Smith 2003; Zank et al. 2018b; Elliott et al. 2019). Both stream-shear and PUI creation convert solar kinetic energy to heat energy. Equation (1), when multiplied by  $U$ , together with the constancy of mass flux, yields

$$\frac{1}{r^2} \frac{d}{dr} \left( \rho U r^2 \frac{U^2}{2} \right) = -U \frac{dP}{dr} - \rho S^{\text{shear}} - \rho S^{\text{PUI}}, \quad (2)$$

and is the momentum equation written in terms of the kinetic energy flux of the solar wind flow. Similarly, the transport equation for the thermal pressure (Zank et al. 2018b),

$$U \frac{dP}{dr} + \gamma \frac{P}{r^2} \frac{d}{dr} (r^2 U) = (\gamma - 1) S_t, \quad (3)$$

can be rewritten as

$$\frac{1}{r^2} \frac{d}{dr} \left( \rho U r^2 \frac{\gamma}{\gamma - 1} \frac{P}{\rho} \right) = U \frac{dP}{dr} + S_t, \quad (4)$$

where  $S_t$  is the turbulence heating term. Adding Equations (2) and (4) yields

$$\frac{1}{r^2} \frac{d}{dr} \left( \rho U r^2 \left( \frac{U^2}{2} + \frac{\gamma}{\gamma - 1} \frac{P}{\rho} \right) \right) = S_t - \rho S^{\text{shear}} - \rho S^{\text{PUI}}. \quad (5)$$

The left-hand side (lhs) of Equation (5) expresses the conservation of kinetic and thermal energy in the solar wind.

However, Equation (5) does not yet represent conservation of total energy since the turbulent energy flux has not yet been included. We combine Equation (5) with the transport equations of the fluctuating magnetic energy density derived in the Appendix (see also, Zank et al. 1996, 2012). In the Appendix, we derived coupled turbulence transport equations for the fluctuating magnetic energy density and the correlation length of the magnetic field fluctuations for the following cases: (i) within 10 au, in which the solar wind turbulence is dominated mainly by the fluctuating magnetic energy (Adhikari et al. 2015, 2017; Zank et al. 2017, 2018b) which corresponds essentially to quasi-2D magnetic turbulence (Zank et al. 2017), and (ii) in the outer heliosphere beyond 10 au, where turbulence driven by PUI creation and isotropization excites Alfvén waves, making the fluctuating magnetic and kinetic energy approximately equal (Adhikari et al. 2015, 2017; Zank et al. 2017, 2018b) which corresponds essentially to slab turbulence (Zank et al. 2017).

For case (i), Equations (17) and (20) are used to describe the transport of the fluctuating magnetic energy density  $E_b^0$  and correlation length  $\lambda_b^0$  of the magnetic field fluctuations described in case (i), respectively. The conservative form of the 1D steady-state transport equation for the quasi-2D fluctuating magnetic energy density  $E_b^0$  (Equation (17)) is given by (see also Zank et al. 1996)

$$\frac{1}{r^2} \frac{d}{dr} (\rho r^2 U E_b^0) = -\rho \frac{E_b^{03/2}}{\lambda_b^0} + \rho C_{\text{sh}} \frac{\Delta U V_{A0}^2 r_0}{r^2}. \quad (6)$$

The first term on the rhs of Equation (6) is the nonlinear term that is responsible for the dissipation of the fluctuating magnetic energy density. Similarly, the transport equation for the correlation length  $\lambda_b^0$  is (see Zank et al. 1996),

$$U \frac{d\lambda_b^0}{dr} = \frac{E_b^{01/2}}{2} - C_{\text{sh}} \frac{\Delta U V_{A0}^2 r_0}{r^2} \frac{\lambda_b^0}{2E_b^0}. \quad (7)$$

For case (ii), Equations (18) and (21) describe the transport equation for the fluctuating magnetic energy density  $E_b^A$  and the correlation length  $\lambda_b^A$ , respectively. The conservative form of the 1D steady-state fluctuating magnetic energy density  $E_b^A$  is given by

$$\frac{1}{r^2} \frac{d}{dr} \left( \rho r^2 U E_b^{A0} \log \left( \frac{\bar{E}_b^A}{\bar{\rho}^{1/2}} \right) \right) = -\rho \frac{\sqrt{2} E_b^{A0} E_b^{A1/2}}{\lambda_b^A} + \frac{\rho E_b^{A0}}{2E_b^A} \frac{f_D n_{\text{H}}^\infty U V_{A0}}{n_{\text{sw}}^0 \tau_{\text{ion}}^0} \exp \left( -\frac{L}{r} \right), \quad (8)$$

where  $\bar{E}_b^A = E_b^A / E_b^{A0}$ ,  $\bar{\rho} = \rho / \rho_0$ ,  $E_b^{A0}$  is the fluctuating magnetic energy density at 1 au, and  $\rho_0$  is the solar wind density at 1 au. Similarly, the 1D steady-state transport equation for the correlation length  $\lambda_b^A$  is

$$U \frac{d\lambda_b^A}{dr} = \frac{E_b^{A1/2}}{\sqrt{2}} - \frac{f_D n_{\text{H}}^\infty U V_{A0}}{n_{\text{sw}}^0 \tau_{\text{ion}}^0} \exp \left( -\frac{L}{r} \right) \frac{\lambda_b^A}{4E_b^A}. \quad (9)$$

Combining Equations (5), (6), and (8) yields

$$\begin{aligned} & \left. \frac{1}{r^2} \frac{d}{dr} \left[ \rho U r^2 \left( \frac{U^2}{2} + \frac{\gamma}{\gamma-1} \frac{P}{\rho} + E_b^0 + E_b^{A0} \log \left( \frac{\bar{E}_b^A}{\bar{\rho}^{1/2}} \right) \right) \right] \right. \\ &= \left( S_t - \rho \frac{E_b^{03/2}}{\lambda_b^0} - \rho \frac{\sqrt{2} E_b^{A0} E_b^{A1/2}}{\lambda_b^A} \right) \\ &+ \rho \left( S^{\text{shear}} - C_{\text{sh}} \frac{r_0 \Delta U V_{A0}^2}{r^2} \right) \\ &+ \rho \left( S^{\text{PUI}} - \frac{E_b^{A0} f_D n_{\text{H}}^{\infty} U V_{A0}}{2 E_b^A n_{\text{sw}}^0 \tau_{\text{ion}}^0} \exp \left( -\frac{L}{r} \right) \right). \end{aligned} \quad (10)$$

To conserve total energy, the rhs of Equation (10) needs to be zero, which implies that

$$\begin{aligned} S_t &= \rho \frac{E_b^{03/2}}{\lambda_b^0} + \rho \frac{\sqrt{2} E_b^{A0} E_b^{A1/2}}{\lambda_b^A}; \quad S^{\text{shear}} = C_{\text{sh}} \frac{r_0 \Delta U V_{A0}^2}{r^2}; \\ S^{\text{PUI}} &= \frac{E_b^{A0} f_D n_{\text{H}}^{\infty} U V_{A0}}{2 E_b^A n_{\text{sw}}^0 \tau_{\text{ion}}^0} \exp \left( -\frac{L}{r} \right). \end{aligned} \quad (11)$$

The first term of Equation (11) is the turbulent heating term (Verdini et al. 2010; Zank et al. 2018b), and the second and third terms are turbulence sources related to shear flow, and PUIs (Zank et al. 2017), and were included in Equation (2). Equation (10) then becomes

$$\begin{aligned} & \frac{1}{r^2} \frac{d}{dr} \left[ \rho U r^2 \left( \frac{U^2}{2} + \frac{\gamma}{\gamma-1} \frac{P}{\rho} + E_b^0 + E_b^{A0} \log \left( \frac{\bar{E}_b^A}{\bar{\rho}^{1/2}} \right) \right) \right] = 0; \\ & \Rightarrow \rho U r^2 \left( \frac{U^2}{2} + \frac{\gamma}{\gamma-1} \frac{P}{\rho} + E_b^0 + E_b^{A0} \log \left( \frac{\bar{E}_b^A}{\bar{\rho}^{1/2}} \right) \right) = \text{const.} \end{aligned} \quad (12)$$

Equation (12) shows that the sum of kinetic flow energy, enthalpy, and the turbulent (magnetic) energy density is conserved. In other words, the large-scale solar wind flow drives stream-shear instabilities and energizes PUIs, and through their isotropization drives further turbulence. In turn, the turbulence energy cascades to small (dissipative) scales to heat the solar wind. This system of energy transfer is closed and hence conservative. In Equation (12), the sum of the third and fourth terms inside the parentheses corresponds to the total fluctuating magnetic energy density throughout the heliosphere. The third term  $E_b^0$  is important within 10 au, and the fourth term  $E_b^{A0} \log(\bar{E}_b^A / \bar{\rho}^{1/2})$  is important beyond 10 au. Thus, Equation (12) simply expresses the transfer of supersonic solar wind energy and momentum into turbulent energy via stream-shear and PUI creation and isotropization, which in turn is dissipated as heat in the solar wind. In Equation (12),  $\rho U r^2$  is the mass flux, which can be expressed in the form

$$\frac{1}{r^2} \frac{d}{dr} (r^2 \rho U) = 0. \quad (13)$$

**Table 1**  
The Symbols Used in the Paper Together with a Brief Description

Solar wind parameters and turbulent quantities	
$S, T, P$	Solar wind entropy, solar wind proton temperature and solar wind thermal pressure
$E_b^0, \lambda_b^0$	Quasi-2D fluctuating magnetic energy density and the corresponding correlation length
$E_b^A, \lambda_b^A$	Slab fluctuating magnetic energy density and the corresponding correlation length
$U, (\rho)n$	Solar wind speed, and solar wind (mass) density
$S_t, S^{\text{shear}}, S^{\text{PUI}}$	Turbulent heating, shear source of turbulence and PUI source of turbulence
$V_{A0}, \Delta U$	Alfvén velocity and difference between the fast and slow solar wind
$n_{\text{sw}}^0, n_{\text{H}}^{\infty}$	Solar wind density at 1 au and neutral hydrogen density
$C_{\text{sh}}, f_D$	Strength of the turbulent shear source and fraction of PUI source generating turbulence
$\alpha, \beta$	von-Kármán–Taylor constant
$E_T, E_D, E_C$	Total turbulent energy, residual energy and cross-helicity
$L^T, L_D$	Correlation function of total turbulent energy and residual energy
$\langle u^2 \rangle, \langle b^2 \rangle, r_A$	Fluctuating kinetic energy, fluctuating magnetic energy and Alfvén ratio
$\lambda^{\pm}, \lambda_D$	Correlation lengths of forward and backward propagating modes, and residual energy

To derive the transport equation for entropy  $S (= c_v \log(P/\rho^\gamma))$ , we combine Equation (3) with (13), which yields

$$U \frac{dS}{dr} = (\gamma - 1) c_v \frac{1}{P} S_t. \quad (14)$$

Equation (14) can be written in a conservative form with turbulent heating,

$$\frac{1}{r^2} \frac{d}{dr} (\rho U r^2 S) = (\gamma - 1) c_v \frac{\rho}{P} S_t. \quad (15)$$

Equations (14) and (15) differ from the entropy conservation equation derived from the ideal MHD equations (Zank 2014) because of the turbulent heating term  $S_t$ . Equations (14) and (15) show that entropy is not conserved in the presence of turbulent dissipation. Both equations show that entropy decreases, when the polytropic index  $\gamma < 1$  (since  $dS/dr < 0$ ), and increases, when the polytropic index  $\gamma > 1$  (since  $dS/dr > 0$ ). We solve the coupled solar wind and turbulence transport equations numerically by a Runge–Kutta 4th order method, and compare the numerical solutions with *Voyager 2* measurements.

### 3. Results

We solve the coupled solar wind and turbulence transport equations using the boundary conditions at 1 au: fluctuating magnetic energy densities  $E_b^0 = 300 \text{ km}^2 \text{ s}^{-2}$  and  $E_b^A = 6.12 \text{ km}^2 \text{ s}^{-2}$ , correlation lengths  $\lambda_b^0 = 0.01 \text{ au}$  and  $\lambda_b^A = 0.03 \text{ au}$ , solar wind proton temperature  $T = 5 \times 10^4 \text{ K}$ , solar wind speed  $U = 420 \text{ km s}^{-1}$ , and solar wind density  $\rho = 7 \text{ cm}^{-3}$ . Similarly, we use  $V_{A0} = 50 \text{ km s}^{-1}$ ,  $\Delta U = 200 \text{ km s}^{-1}$ ,  $C_{\text{sh}} = 0.25$ ,  $f_D = 0.4$ ,  $n_{\text{H}}^{\infty} = 0.1 \text{ cm}^{-3}$ ,  $\tau_{\text{ion}}^0 = 10^6 \text{ s}$ ,  $n_{\text{sw}}^0 = 7 \text{ cm}^{-3}$ ,

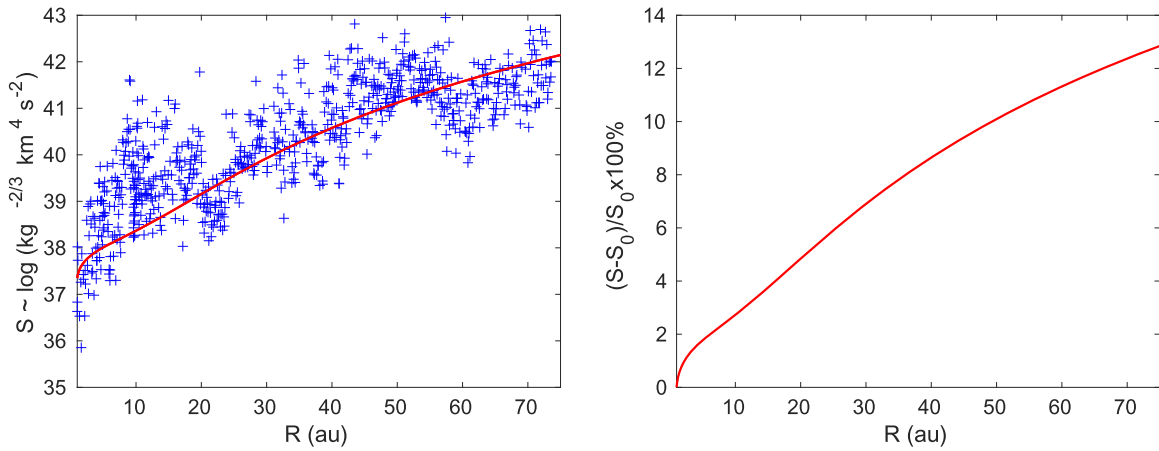


**Figure 1.** Left: comparison of the theoretical (solid curve) and observed entropy (blue “+” symbols) as a function of heliocentric distance. Right: percentage increase in entropy with heliocentric distance.

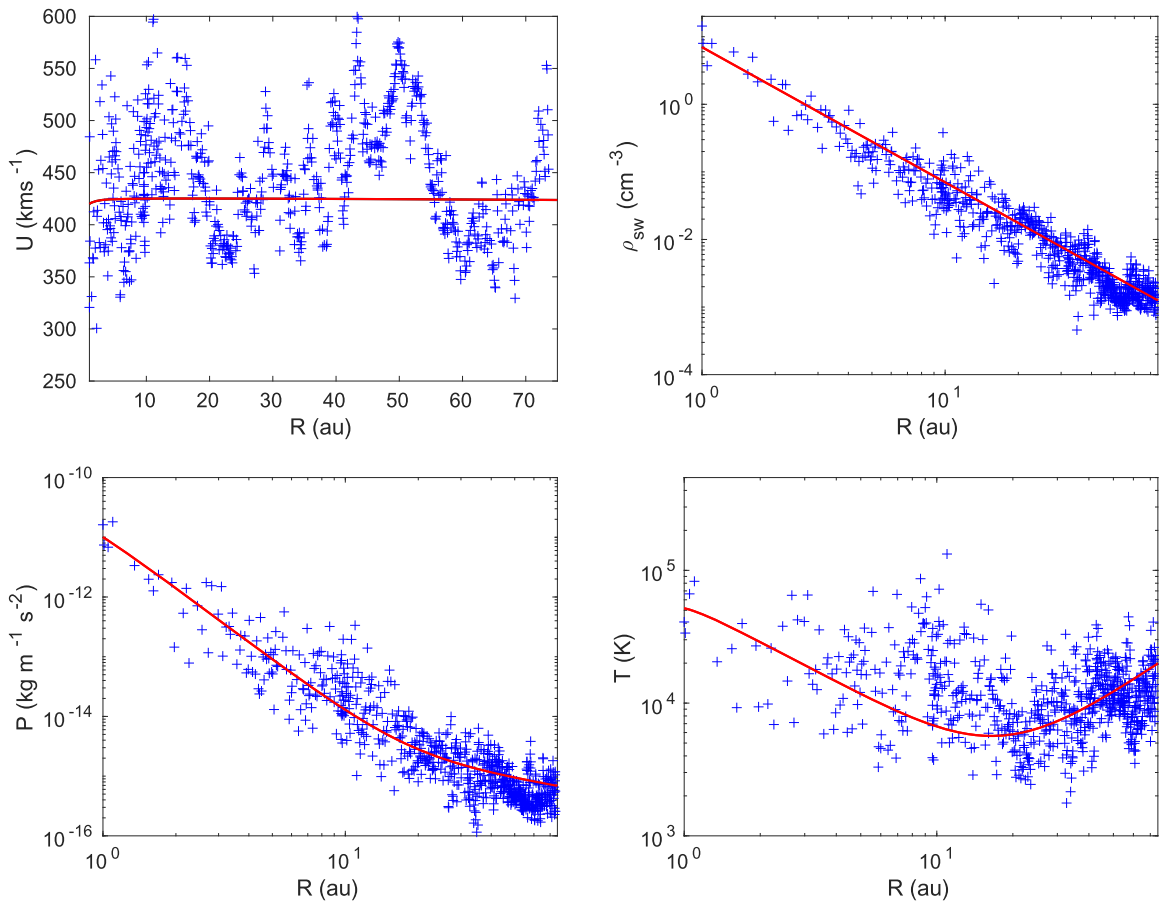


**Figure 2.** The solar wind variables as a function of heliocentric distance. Top left: solar wind speed. Top right: solar wind density. Bottom left: thermal gas pressure. Bottom right: solar wind temperature. Red curves are theoretical results, and blue plus symbols are observed results from Adhikari et al. (2017).

and  $L = 7$  au. Symbols used in the manuscript are listed in Table 1.

We compare the theoretical results with *Voyager 2* measurements. To calculate the theoretical and observed entropy, we use  $S \sim \log(P/\rho^\gamma)$ .

To derive the observed solar wind entropy, we use the solar wind thermal pressure  $P$  and the solar wind (mass) density shown in Figure 2, and we use a polytropic index of  $\gamma = 5/3$ . The observed results are taken from Adhikari et al. (2017), in which each value corresponds to 500 hr. The left panel of

Figure 1 shows the comparison of the theoretical and observed entropy as a function of heliocentric distance. In the left panel of Figure 1, the red curve corresponds to the theoretical solar wind entropy, and the scattered blue “+” symbol is the observed entropy. The observed and theoretical entropy increase with increasing heliocentric distance, and are consistent with each other between 1 and 75 au. The dissipation of turbulence leads to an increase in the solar wind entropy. The coincidence of theoretical and observed values of  $S$  in Figure 1 derives from the theoretical and observed values of  $P$  and  $\rho$

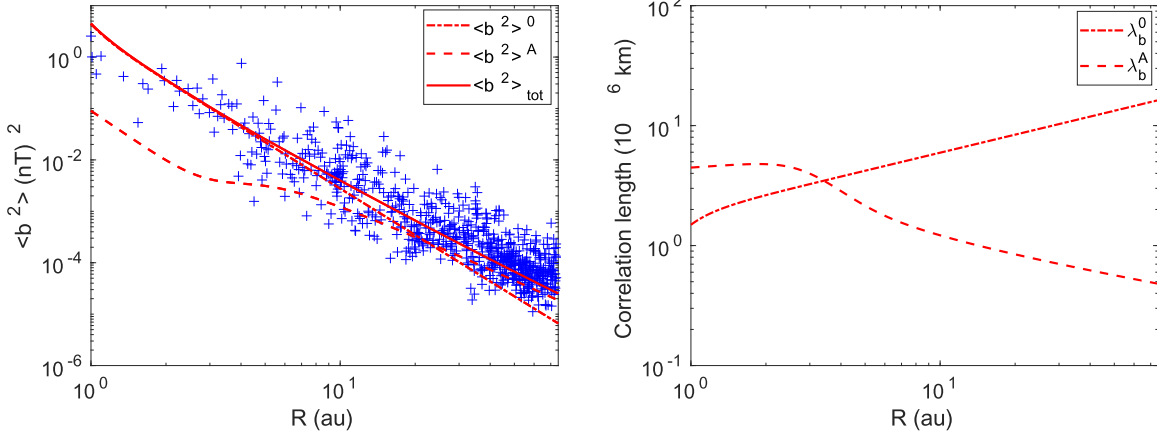


**Figure 3.** Left: comparison between the theoretical and observed fluctuating magnetic energy as a function of heliocentric distance. Right: correlation length of the fluctuating magnetic energy as a function of distance. See text for details.

shown in Figure 2. The right panel of Figure 1 shows the percentage change in entropy  $(S - S_0)/S_0 \times 100\%$ , where  $S_0$  is the solar wind entropy at 1 au, with increasing heliocentric distance, indicating that the entropy at 75 au increased by about 12.84% compared to its value at 1 au. This entropy increase is due to the dissipation of turbulence exclusively and possible contributions to temporal effects such as shock waves as excluded. Based on the agreement of theory and observations, it would appear that the dissipation is largely responsible for the observed increase in entropy from 1 to 75 au.

Figure 2 shows the solar wind speed (top left), solar wind density (top right), thermal pressure (bottom left), and solar wind proton temperature (bottom right) as a function of heliocentric distance. Since the solar wind and turbulence transport equations are coupled, the solution shown in Figure 2 is affected by the turbulent energy density and the correlation length shown in Figure 3, and vice versa. In the figure, the solid curves are the theoretical results and the plus symbols are observations. In the top left panel of Figure 2, the theoretical solar wind speed increases slightly initially because of the pressure gradient. Thereafter, the solar wind speed decreases slightly as the energy of the solar wind flow is removed by stream-shear and PUIs. The decrease in the solar wind speed is not as obvious as in Zank et al. (2018b), in which the solar wind speed decreases by about 14.77% at 75 au (see also, Richardson & Smith 2003; Elliott et al. 2019). However, we note that the solar wind speed is derived from the conservative solar wind and turbulence transport equations, in which the total (solar wind plus turbulent) energy flux is constant (see Equation (12)). The variation in the observed solar wind speed between  $\sim 350$  and  $\sim 550$  km s $^{-1}$  is caused by the solar cycle.

The top right panel of Figure 2 displays the solar wind density  $\rho_{sw}$  as a function of heliocentric distance. The theoretical and observed solar wind density exhibit similar radial profiles with increasing heliocentric distance. The bottom left and right panels of Figure 2 are the thermal gas pressure and the solar wind proton temperature, showing that the theoretical and observed thermal pressure and proton temperature are in good agreement with distance.

The left panel of Figure 3 shows the comparison between the theoretical and observed fluctuating magnetic energy as a function of heliocentric distance. The theoretical  $\langle b^2 \rangle^{0,A}$  is derived from  $E_b^{0,A} = \langle b^2 \rangle^{0,A} / \mu_0 \rho$ , where  $\mu_0$  is the magnetic permeability. In the figure, the dashed curve describes the

fluctuating magnetic energy associated with PUI-driven turbulence, the dashed-dotted-dashed curve describes the fluctuating magnetic energy associated with solar wind turbulence dominated by the fluctuating magnetic energy, and the solid curve represents their sum. The dashed curve initially decreases, then flattens, and then decreases with increasing heliocentric distance. The rate of energy decrease beyond  $\sim 10$  au is slower than that within  $\sim 3$  au. The flattening and the slow decrease of the dashed curve is due to the generation of PUI-driven turbulence in the outer heliosphere. The dashed-dotted-dashed and solid curve decrease in a similar manner until  $\sim 5$  au, and then the dashed-dotted-dashed curve decreases faster than the solid curve with increasing heliocentric distance. The PUI-driven turbulence dashed curve is initially very small compared to the stream-shear-driven turbulence curve, and then becomes larger beyond  $\sim 10$  au when PUI-driven turbulence dominates and the stream-shear source becomes negligible.

The right panel of Figure 3 shows the theoretical correlation length of magnetic field fluctuations as a function of heliocentric distance. The dashed-dotted-dashed curve shows the correlation length  $\lambda_b^0$  of the fluctuating quasi-2D magnetic energy  $\langle b^2 \rangle^0$ , and the dashed curve indicates the correlation  $\lambda_b^A$  of the fluctuating slab magnetic energy  $\langle b^2 \rangle^A$ . The correlation length  $\lambda_b^0$  increases gradually with distance, while the  $\lambda_b^A$  initially increases slightly, and then decreases with increasing heliocentric distance due to the PUI source of turbulence.

#### 4. Discussion and Conclusions

In this paper, we derived conservative coupled solar wind and turbulence transport model equations, and studied the evolution of entropy between 1 and 75 au. We showed that the solar wind flow energy drives turbulence generated by both stream-shear and PUI creation and isotropization, which is then dissipated as heat back into the solar wind. Both stream-shear and PUI creation leads to a decrease of the solar wind speed (Richardson & Smith 2003; Zank et al. 2018b; Elliott et al. 2019). Compared with the conserved entropy equation derived from the ideal MHD equations (Zank 2014), the entropy transport equation derived in this paper acquires a turbulent heating source term, indicating that the entropy is not conserved. Entropy only increases for an adiabatic index satisfying  $\gamma > 1$ . We also derived the coupled turbulence transport equations for the

fluctuating magnetic energy density and the correlation length of the magnetic field fluctuations for two cases: (i) when the solar wind fluctuations are dominated mainly by the fluctuating quasi-2D magnetic energy, and (ii) when the turbulence driven by PUI excites Alfvén waves, in which case the fluctuating kinetic and magnetic energy become approximately equal (slab turbulence). In the former case, the turbulence transport model equation includes a stream-shear source of turbulence, and in the latter case, the turbulence transport model equation includes the PUI source of turbulence.

We solved the coupled solar wind and turbulence transport equations from 1 to 75 au, and compared the theoretical solution with measured values derived from *Voyager 2* observations. The results are summarized as follows.

1. The sum of the solar wind and turbulent magnetic energy flux is constant.
2. The theoretical and observed solar wind entropy increases with increasing heliocentric distance in a similar manner. The entropy at 75 au is about 12.84% larger than that at 1 au.
3. Fluctuating quasi-2D magnetic energy driven by stream-shear decreases monotonically with increasing heliocentric distance, whereas, the slab turbulence driven by PUIs is negligible within  $\sim 3\text{--}7$  au, and then, although dominant in the outer heliosphere decreases with increasing heliocentric distance. The theoretical total fluctuating magnetic energy follows a very similar profile to that of the observed fluctuating magnetic energy.
4. The theoretical and observed solar wind proton temperature decreases until  $\sim 20$  au, and then increases with increasing heliocentric distance due to the dissipation of PUI-driven turbulence. Agreement between the model and observations is very good.
5. The theoretical and observed solar wind density decreases with increasing heliocentric distance, and are in good agreement between 1 and 75 au.

By combining the solar wind equations with the turbulent transport equations for the fluctuating magnetic energy density, the total energy flux (i.e., the sum of solar wind energy flux, enthalpy, and turbulent (magnetic) energy flux) is shown to be constant. This model can be further refined by using the recently developed nearly incompressible MHD turbulence transport model equations (Zank et al. 2017), and it would be worth extending to solar corona and comparing the results with the Parker Solar Probe measurements.

We acknowledge the partial support of NASA grants NNX 08AJ33G, Subaward 37102-2, NNX14AC08G, the PSP contract SV4-84017, an NSF-DOE grant PHY-1707247, and the partial support of NSF EPSCoR RII-Track-1 cooperative agreement OIA-1655280.

## Appendix

### Derivation of the Turbulence Transport Equations

Here, we derive transport equations for the fluctuating magnetic energy density and correlation length for two cases. (i) In the region from 1 to 10 au, solar wind fluctuations are dominated mainly by the fluctuating quasi-2D magnetic energy (Adhikari et al. 2015, 2017; Zank et al. 2017, 2018b). Over this region, we may therefore assume  $\langle u^2 \rangle \sim 0$ ,  $\langle b^2 \rangle / \mu_0 \rho \equiv E_b^0 \neq 0$ , and  $E_D / E_T = -1$ . (ii) PUI-driven

turbulence corresponds to excited Alfvén waves in the outer heliosphere beyond 10 au (Zank et al. 1996, 2017, 2018b; Adhikari et al. 2015, 2017), ensuring that the fluctuating kinetic and magnetic energy are approximately equal, i.e., the residual energy  $E_D \sim 0$ . Case (ii) corresponds to slab turbulence. In both cases, we assume that the cross-helicity is zero ( $E_C = 0$ ). Under this assumption, the transport equation for the total turbulent energy  $E_T$ , Equation (37) of Zank et al. (2012), can be written as

$$\frac{\partial E_T}{\partial t} + \mathbf{U} \cdot \nabla E_T + \frac{1}{2} \nabla \cdot \mathbf{U} E_T + \left( 2a - \frac{1}{2} \right) \times \nabla \cdot \mathbf{U} E_D = -\frac{E_T^{3/2}}{\lambda_+} - \frac{E_T^{3/2}}{\lambda_-} + S_1, \quad (16)$$

where  $\lambda_+$  and  $\lambda_-$  are the correlation lengths corresponding to the forward and backward propagating modes, respectively, and  $S_1$  is a source of turbulence. The total turbulent energy is the sum of the fluctuating kinetic and magnetic energy, i.e.,  $E_T = \langle u^2 \rangle + E_b$ , and the residual energy is the difference between the fluctuating kinetic and magnetic energy, i.e.,  $E_D = \langle u^2 \rangle - E_b$ .

For case (i), since the fluctuating kinetic energy is zero, the fluctuating magnetic energy can be regarded as the total turbulent energy. As a result,  $E_T = E_b^0$ , and  $E_D = -E_b^0$ . Hence, Equation (16) with  $a = 1/2$  (Zank et al. 2012) can be written in the form

$$\frac{\partial E_b^0}{\partial t} + \mathbf{U} \cdot \nabla E_b^0 = -\frac{E_b^{03/2}}{\lambda_+} - \frac{E_b^{03/2}}{\lambda_-} + S_1 \equiv -\alpha \frac{E_b^{03/2}}{\lambda_b^0} + C_{\text{sh}} \frac{r_0 \Delta U V_{A0}^2}{r^2}, \quad (17)$$

where  $\lambda_b^0$  is the correlation of  $E_b^0$ . The second term on the rhs is the shear source of turbulence (Zank et al. 2017). The parameter  $C_{\text{sh}}$  is the strength of the turbulent shear source,  $\Delta U$  is the difference between the fast and slow solar wind, and  $V_{A0}$  is the Alfvén velocity at a reference distance  $r_0$ . Equation (17) assumes the total fluctuating energy of the solar wind within 10 au resides primarily in quasi-2D magnetic field fluctuations, and only includes a shear source of turbulence. Since the turbulent shear source is reduced by  $1/r^2$ , even if we solve Equation (17) from 1 to 75 au, its effect at large distances is negligible. At a large heliocentric distances, however, PUI driving of turbulence is effective. We derive another coupled turbulent transport equation that describes the PUI-driven slab turbulence. For this, we consider case (ii). For case (ii), we can write  $\langle u^2 \rangle = \langle b^2 \rangle / \mu_0 \rho \equiv E_b^A$ ,  $r_A = 1$ , and  $E_D^A = 0$ , so that  $E_T^A = 2E_b^A$ . Then, Equation (16) becomes

$$\frac{\partial E_b^A}{\partial t} + \mathbf{U} \cdot \nabla E_b^A + \frac{1}{2} \nabla \cdot \mathbf{U} E_b^A = -\alpha \sqrt{2} \frac{E_b^{A3/2}}{\lambda_b^A} + \frac{1}{2} \frac{f_D n_{\text{H}}^{\infty} U V_{A0}}{n_{\text{sw}}^0 \tau_{\text{ion}}^0} \exp\left(-\frac{L}{r}\right), \quad (18)$$

where  $\lambda_b^A$  is the correlation length corresponding to  $E_b^A$ . The second term on the rhs is the PUI source of turbulence. The parameter  $L$  is the ionization cavity length scale,  $n_{\text{H}}^{\infty}$  is the neutral hydrogen density entering the supersonic solar wind,  $n_{\text{sw}}$

is the solar wind density at 1 au,  $\tau_{\text{ion}}^0$  is the neutral H ionization time at 1 au, and  $f_D$  denotes the fraction of PUI source that generates turbulence (Isenberg 2005). At 1 au, the fluctuating magnetic energy  $E_b^A$  is very small. When the PUI source of turbulence begins to dominate the solar wind turbulence in the distant heliosphere, the magnetic energy  $E_b^A$  becomes effective.

We need to derive transport equations for the correlation lengths  $\lambda_b^0$  and  $\lambda_b^A$  to close the transport Equations (17) and (18). For this reason, we consider the transport equation for the total covariance  $L^T$ , Equation (D2) of Zank et al. (2012). Again, by assuming  $E_C = 0$  and neglecting the mixing term in Equation (D2) of Zank et al. (2012), we can write

$$\begin{aligned} \frac{\partial L^T}{\partial t} + \mathbf{U} \cdot \nabla L^T + \frac{1}{2} \nabla \cdot \mathbf{U} L^T \\ + 2 \left( a - \frac{1}{4} \right) \nabla \cdot \mathbf{U} L^D = 0, \end{aligned} \quad (19)$$

where  $L^D (= E_D \lambda_D)$  is the correlation function for the residual energy. The parameter  $\lambda_D$  is the correlation length of the residual energy. For case (i), let us write  $L^D = \lambda_D E_D = -E_b^0 \lambda_D^0 \sim -2E_b^0 \lambda_b^0$  (since we assume  $\lambda_D^0 \sim 2\lambda_b^0$ ) and  $L^T = E^T \lambda^T = (1 + r_A) E_b^0 \lambda_T^0 = 2E_b^0 \lambda_b^0$  since  $r_A = \langle u^2 \rangle / E_b \sim 0$  and assuming  $\lambda_T^0 \sim 2\lambda_b^0$ . Then, Equation (19) can be written in the form

$$\begin{aligned} \frac{\partial \lambda_b^0}{\partial t} + \mathbf{U} \cdot \nabla \lambda_b^0 = \beta \left( E_b^{01/2} - C_{\text{sh}} \frac{r_0 \Delta UV_{A0}^2 \lambda_b^0}{r^2 E_b^0} \right) \\ = \frac{E_b^{01/2}}{2} - C_{\text{sh}} \frac{r_0 \Delta UV_{A0}^2 \lambda_b^0}{r^2 2E_b^0}, \end{aligned} \quad (20)$$

where  $\alpha = 2\beta = 1$  is the von-Kármán–Taylor constant. Similarly, for case (ii), let us write  $L^D = E_D \lambda_D = 0$  and  $L^T = E_T \lambda^T = (1 + r_A) E_b^A \lambda_T^A \sim 4E_b^A \lambda_b^A$ . Then, Equation (19) can be written in the form

$$\begin{aligned} \frac{\partial \lambda_b^A}{\partial t} + \mathbf{U} \cdot \nabla \lambda_b^A \\ = \beta \left( \sqrt{2} E_b^{A1/2} - \frac{f_D n_H^\infty UV_{A0}}{n_{\text{sw}}^0 \tau_{\text{ion}}^0} \exp\left(-\frac{L}{r}\right) \frac{\lambda_b^A}{2E_b^A} \right) \\ = \frac{E_b^{A1/2}}{\sqrt{2}} - \frac{f_D n_H^\infty UV_{A0}}{n_{\text{sw}}^0 \tau_{\text{ion}}^0} \exp\left(-\frac{L}{r}\right) \frac{\lambda_b^A}{4E_b^A}, \end{aligned} \quad (21)$$

which is the transport equation for the correlation length  $\lambda_b^A$ .

### ORCID iDs

L. Adhikari  <https://orcid.org/0000-0003-1549-5256>  
G. P. Zank  <https://orcid.org/0000-0002-4642-6192>  
L.-L. Zhao  <https://orcid.org/0000-0002-4299-0490>  
G. M. Webb  <https://orcid.org/0000-0002-0617-9502>

### References

- Adhikari, L., Zank, G. P., Bruno, R., et al. 2015, *ApJ*, 805, 63  
Adhikari, L., Zank, G. P., Hu, Q., & Dosch, A. 2014, *ApJ*, 793, 52  
Adhikari, L., Zank, G. P., Hunana, P., et al. 2017, *ApJ*, 841, 85  
Anand, R. K., & Yadav, H. C. 2014, *ThCFD*, 28, 369  
Breech, B., Matthaeus, W. H., Minnie, J., et al. 2008, *JGRA*, 113, 8105  
Chandran, B. D. G., & Hollweg, J. V. 2009, *ApJ*, 707, 1659  
Chandran, B. D. G., Li, B., Rogers, B. N., Quataert, E., & Germaschewski, K. 2010, *ApJ*, 720, 503  
Chhiber, R., Subedi, P., Usmanov, A. V., et al. 2017, *ApJS*, 230, 21  
Cranmer, S. R., & van Ballegooijen, A. A. 2010, *ApJ*, 720, 824  
Cranmer, S. R., van Ballegooijen, A. A., & Edgar, R. J. 2007, *ApJS*, 171, 520  
Cranmer, S. R., van Ballegooijen, A. A., & Woolsey, L. N. 2013, *ApJ*, 767, 125  
Dmitruk, P., Matthaeus, W. H., Milano, L. J., et al. 2002, *ApJ*, 575, 571  
Dmitruk, P., Milano, L. J., & Matthaeus, W. H. 2001, *ApJ*, 548, 482  
Elliott, H. A., McComas, D. J., Zirnstein, E. J., et al. 2019, *ApJ*, 885, 156  
Fahr, H. J., & Siewert, M. 2015, *A&A*, 576, A100  
Isenberg, P. A. 2005, *ApJ*, 623, 502  
Livadiotis, G. 2018a, *Entrp*, 20, 799  
Livadiotis, G. 2018b, *EL*, 122, 50001  
Livadiotis, G., & Desai, M. I. 2016, *ApJ*, 829, 88  
Livadiotis, G., & McComas, D. J. 2012, *ApJ*, 749, 11  
Livadiotis, G., & McComas, D. J. 2013, *JGRA*, 118, 2863  
Matthaeus, W. H., Zank, G. P., Oughton, S., Mullan, D. J., & Dmitruk, P. 1999a, *ApJL*, 523, L93  
Matthaeus, W. H., Zank, G. P., Smith, C. W., & Oughton, S. 1999b, *PhRvL*, 82, 3444  
Nicolaou, G., Livadiotis, G., & Moussas, X. 2014, *SoPh*, 289, 1371  
Nicolaou, G., McComas, D. J., Bagenal, F., Elliott, H. A., & Wilson, R. J. 2015, *P&SS*, 119, 222  
Oughton, S., Matthaeus, W. H., Dmitruk, P., et al. 2001, *ApJ*, 551, 565  
Richardson, J. D., & Smith, C. W. 2003, *GeoRL*, 30, 1206  
Shiota, D., Zank, G. P., Adhikari, L., et al. 2017, *ApJ*, 837, 75  
Smith, C. W., Isenberg, P. A., Matthaeus, W. H., & Richardson, J. D. 2006, *ApJ*, 638, 508  
Smith, C. W., Matthaeus, W. H., Zank, G. P., et al. 2001, *JGR*, 106, 8253  
Suzuki, T. K., & Inutsuka, S.-i. 2005, *ApJL*, 632, L49  
Usmanov, A. V., Matthaeus, W. H., Breech, B. A., & Goldstein, M. L. 2011, *ApJ*, 727, 84  
van Ballegooijen, A. A., & Asgari-Targhi, M. 2016, *ApJ*, 821, 106  
van Ballegooijen, A. A., Asgari-Targhi, M., Cranmer, S. R., & DeLuca, E. E. 2011, *ApJ*, 736, 3  
Verdini, A., Velli, M., Matthaeus, W. H., Oughton, S., & Dmitruk, P. 2010, *ApJL*, 708, L116  
Viñas, A. F., Wong, H. K., & Klimas, A. J. 2000, *ApJ*, 528, 509  
Wang, Y. C., Behannon, K. W., Burlaga, L. F., & Zhang, S. 1989, *JGR*, 94, 2345  
Wang, Y. C., Liu, S., & Burlaga, L. F. 1990, *JGR*, 95, 18769  
Wiengarten, T., Oughton, S., Engelbrecht, N. E., et al. 2016, *ApJ*, 833, 17  
Woolsey, L. N., & Cranmer, S. R. 2014, *ApJ*, 787, 160  
Zank, G. P. 2014, in *Transport Processes in Space Physics and Astrophysics*, ed. G. P. Zank (Berlin: Springer)  
Zank, G. P., Adhikari, L., Hunana, P., et al. 2017, *ApJ*, 835, 147  
Zank, G. P., Adhikari, L., Hunana, P., et al. 2018a, *ApJ*, 854, 32  
Zank, G. P., Adhikari, L., Zhao, L. L., et al. 2018b, *ApJ*, 869, 23  
Zank, G. P., Dosch, A., Hunana, P., et al. 2012, *ApJ*, 745, 35  
Zank, G. P., Matthaeus, W. H., Bieber, J. W., & Moraal, H. 1998, *JGR*, 103, 2085  
Zank, G. P., Matthaeus, W. H., & Smith, C. W. 1996, *JGR*, 101, 17093  
Zhao, L. L., Adhikari, L., Zank, G. P., Hu, Q., & Feng, X. S. 2017, *ApJ*, 849, 88  
Zhao, L.-L., Adhikari, L., Zank, G. P., Hu, Q., & Feng, X. S. 2018, *ApJ*, 856, 94